JMST Advances (2020) 2:1–8
https://doi.org/10.1007/s42791-020-00029-1

Online ISSN 2524-7913
Print ISSN 2524-7905

LETTER

Mathematical modeling and finite element analysis of the mechanical behavior of hybrid structures in complex materials

Salah Aguib[1]

Received: 29 September 2019 / Revised: 11 December 2019 / Accepted: 31 January 2020 / Published online: 2 March 2020

Abstract

In this research work, the mechanical behavior of a hybrid sandwich beam in magnetorheological elastomer loaded with 40% ferromagnetic particles has been studied. A finite element model has been developed for the three layers. The sandwich beam is modeled using transverse displacement at core layer. The finite element model of the damped three-layer beam is assumed that every layer has the same transverse displacement, and it is derived using the Golla–hughes–McTavish's principle. Different specimens have been modeled by varying the magnetic field intensity and static force and studied under the clamped-free and cantilever boundary conditions for modal analysis. Results show the influence of MRE adaptive stiffness and the loss factor in the static behavior of the sandwich studied. The structure proposed can be directly applied to civil engineering, for example, aeronautics, aerospace, and building foundations.

Graphical Abstract

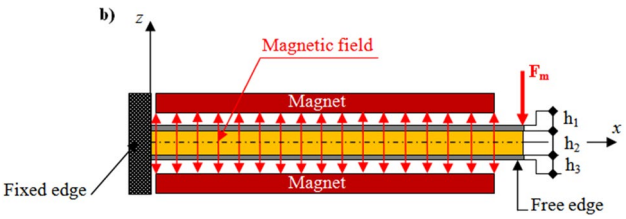

Keywords Mechanical behavior · MRE hybrid sandwich · Mathematical modeling · Finite element analysis · Magnetic field

1 Introduction

The importance of constructions (nuclear centrals, space structures, etc.) is continuously increasing because of developing technology. Materials are generally accepted as elastic in engineering constructions due to calculation simplicity. But, used materials actually demonstrate a viscoelastic nonlinear behavior. So, models which give the actual behavior of material with more time-consuming computing capacity should be used for more precise determination of behavior of materials used in constructions. This requires competitive mathematical models. In metals, the modulus of elasticity can be modeled as a constant. On the other hand, the modulus of elasticity of complex materials is variable and they are modeled by functions. The magnetorheological elastomers (MRE) consist of ferromagnetic particles (generally of micrometric size) dispersed in a silicone elastomeric matrix.

Zhou and Wang [1] formulated an analytical model of the vibrating motion of a sandwich beam under a uniform magnetic field, perpendicular to the direction of the thickness. To validate the analytical model, they conducted a second study based on numerical modeling to control the rheological properties. Dwivedy et al. [2] studied the parametric instability areas of a sandwich beam with a magnetorheological elastomer core. Wan et al. [3] performed dynamic mechanical analysis tests to determine the viscoelastic properties of MRE under different conditions. The results found

✉ Salah Aguib
s.aguib@univ-boumerdes.dz

[1] Dynamic of Engines and Vibroacoustic Laboratory, Department of Mechanical Engineering, F.T, M.B. Boumerdes University, Boumerdes, Algeria

show that the transition behavior of MRE samples based on silicon rubber under uniaxial compression occurs at about 50 °C. The storage modulus presents two different trends with temperature variation: it first decreases rapidly then increases slightly or maintain a stable value as the temperature increases. In their work, Bastola et al. [4] have used a 3D printing technology suitable for the development of a magnetorheological elastomer (MRE) by multi-material printing and where the MR fluid volume is encapsulated in a layer-by-layer elastomeric matrix. The choice of printing materials determines the final structure of the 3D-printed hybrid MR elastomer. Experimental results and forced vibration tests show that 3D-printed MR elastomers could change their elasticity and damping properties when exposed to the external magnetic field. In addition, the 3D-printed MR elastomer also exhibits anisotropic behavior when the direction of the magnetic field is changed with respect to the orientation of the printed filaments. Yao et al. [5] developed a new magnet-induced aligning magnetorheological elastomer (MIMRE) based on an ultra-soft polymer matrix. This synthetic production method allows the magnetic particles to move and align in an elastomeric matrix under a magnetic field at room temperature. They found that the MIMRE has excellent properties under the effect of the magnetic field. Touron et al. [6] represented a helicopter flight energy control; this representation is considered to be an operator support system for Port Hamiltonian. Generic sufficient conditions are given on the assistance location and structure which allow the assisted system to be dissipative, hence, providing nice stability and power scaling properties. Results are applied to the design of assistance for a simplified flight control system. Simulations show the relevance of the method and are compared to real-life results. Dargahi et al. [7] were based primarily on a thorough experimental characterization of the static and dynamic properties of different types of magnetorheological elastomers. To this end, six different types of MRE samples with varying contents of ferromagnetic particles have been manufactured. Akhavan et al. [8] considered the effects of Casimir force and the magnetic field on the tensile instability of a MEMS cantilever sandwich actuator in a magnetorheological elastomeric sandwich with conductive skins. The basic equations and the corresponding boundary conditions are obtained by the variational principle based on Euler–Bernoulli beam theory. These last equations are solved by the generalized differential quadrature method (GDQM). The results found show a decrease in the deflection of the moving electrode, which causes instability of the electrode at higher voltages, that is, as the magnetic field increases, the tensile stress also increases. The study by Dargahi et al. [9] presents a Prandtl–Ishlinskii model based on a stop operator to predict the nonlinear hysteresis properties of MRE as a function of strain amplitude, excitation frequency and magnetic field density. The stress–strain properties of an MRE with 40% of iron particles were experimentally determined in shear mode over wide ranges of strain amplitudes (2.5–20%), excitation frequencies (0, 1–50 Hz) and magnetic flux densities (0–450 mT). In this study, Lai et al. [10] prepared MRE based on natural rubber and carbonyl iron particles. They used the Taguchi method to study the effect of several dominant factors during the manufacturing process, such as the pre-hardening time, pre-hardening temperature, and the magnetic field applied during hardening on the post-hardening loss factor and tensile properties. The loss factor was measured using a parallel plate rheometer in a frequency range of 1–100 Hz and a range of strain amplitudes from 0.1 to 6%. The tensile properties were measured with a universal tensile testing machine. The results found indicate that the magnetic field has a large influence on the loss factor when measured over a range of frequency and elongation at rupture. In this paper, Xing et al. [11] modeled the dynamic and vibration control of a two-blade propeller system of an aircraft in the presence of input magnitude and rate constraints and external disturbances. To avoid discretizing the original system, a partial differential equation (PDE) model preserving all system modes is developed. On this basis the proposed PDE model, boundary control laws are derived to restrict the bending and twist deformations of the two-blade propeller under disturbances. Numerical simulations are presented to demonstrate the effectiveness of the proposed control method.

The main purpose of this paper is to model new hybrid smart structures suitable for a wide range of working conditions. To do this, we have developed a numerical code in the Matlab to determine the static behavior of beams having different materials by the finite element method. To guarantee a good continuity and the transition of the movements and stress at the interfaces between different parts of the beam, we have used a hybrid mesh.

2 Geometrical modeling and mathematical formulation of hybrid sandwich beam

2.1 Geometrical modeling

The sandwich beam model described here is based on the following assumptions:

- Top and bottom layers are considered as ordinary beams with axial and bending resistance.
- The core layer carries negligible longitudinal stress, but takes the non-linear displacement fields in x- and z-directions.
- Transverse displacements of top and bottom layers equal transverse displacement of core at the sandwich beam

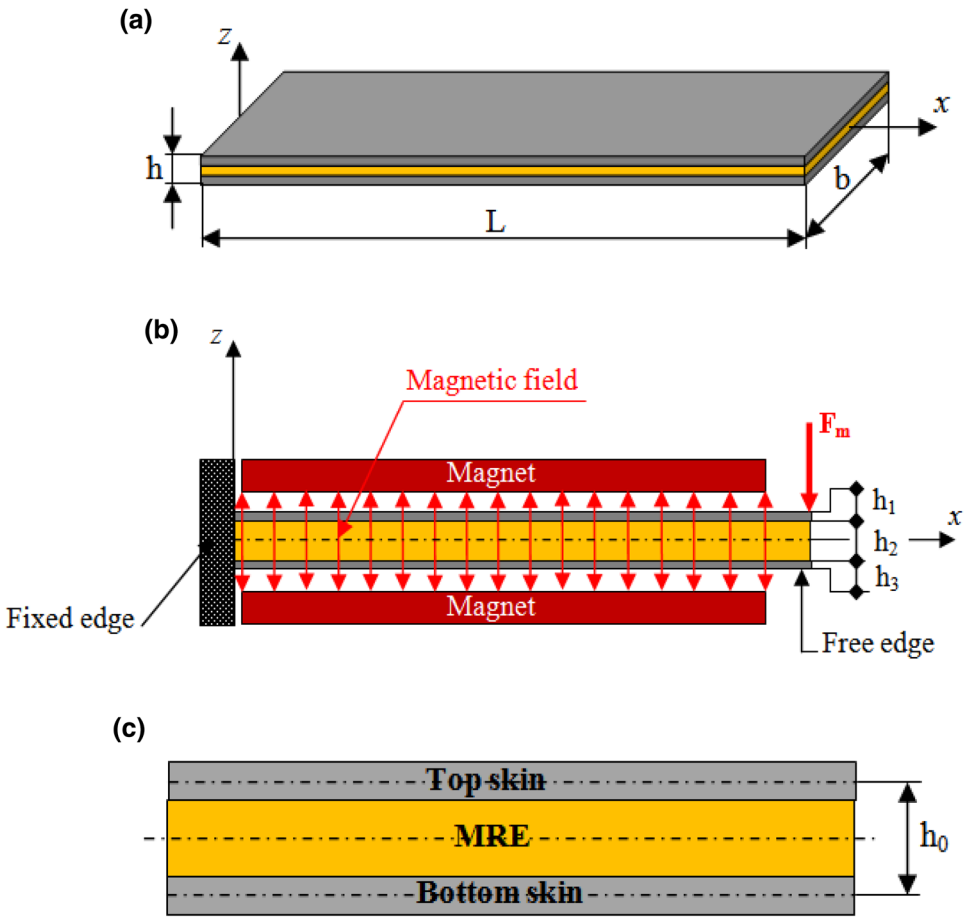

Fig. 1 Magnetorheological hybrid sandwich beam model

considered here consisting of three layers with viscoelastic material as a core layer, the top and bottom layers are isotropic and linear elastic material with thickness h_1 and h_3. The magnetorheological elastomer (MRE) core layer has a thickness of h_2, the complex shear modulus in the form of $G_c = G' + iG''$ where η is the loss factor. The model of the magnetorheological sandwich beam has been shown in Fig. 1a–c.

2.2 Mathematical modeling

The bending and membrane strains of the aluminum layers and the shear strain of the MRE are considered in the following formulation. The bending and membrane effects of the MRE neglected as it is considered and proved in earlier works by Tezcan [12] and Zhang [13]. The beam is subjected to magnetoelastic load and to concentrated magnetic load at its clamped extremity. In static domain, the principle of virtual works is given by

$$\delta P_{\text{ext}} + \delta P_{\text{int}} = 0, \tag{1}$$

δP_{int} denotes the virtual works of the internal forces. Their expressions are given by

$$\delta P_{\text{int}} = \int_0^L \left[EIw_{,xx}\delta w_{,xx} + N_1\delta u_{1,x} + N_3\delta u_{3,x} + (N_1 + N_2)w_{,x}\delta w_{,x} + G_c bh_2\gamma_c\delta\gamma_c \right] \mathrm{d}x, \tag{2}$$

where δu_1, δu_3, δw and $\delta\gamma_c$ denotes the virtual displacements and the virtual shear strain, in Eq. (2) $(N_1 + N_2)w_{,x}$ represents the non-linear term. In Eq. (2), N_1, N_3 and γ_c are the axial forces in the top and bottom layers and the shear strain in the MRE layer given by

$$N_1 = EA_1\left(u_{1,x} + \frac{1}{2}(w_{,x})^2\right),$$

$$N_3 = EA_3\left(u_{3,x} + \frac{1}{2}(w_{,x})^2\right), \tag{3}$$

$$\gamma_c = \frac{u_1 - u_3}{h_2} + \frac{h_0}{h_2}w_{,x},$$

where A_1 and A_3 are the cross area of top and bottom aluminum ply, the sum of quadratic moments of the two aluminum layers.

δP_{ext} denotes the virtual works of the internal forces. Their expressions are given by

$$\delta P_{\text{ext}} = -\int_0^L \left(q_1\delta w + n_1\delta u_1 + m_1\delta w_{,x} + q_3\delta w + n_3\delta u_3 + m_3\delta w_{,x}\right)\mathrm{d}x + F_m\delta w(0), \tag{4}$$

where q_i, n_i and $m_i (i = 1, 3)$ are the vertical, horizontal and moments external distributed loads, respectively, at top (t) and bottom (b) skins and F_m is the magnetic force applied to the free edge beam:

$$F_m = B_r \times \nabla H \times V, \tag{5}$$

where B_{r} is the remanent induction related to the remanent magnetization, ∇H is the gradient of magnetic field, or the magnetoelastic loads applied to the conductive beam will be equivalent to the following horizontal force distribution and the distributed moments are expressed as

$$n_i^m = n_i^{\text{Lor}} = \frac{B_0^2 b h_i}{\mu_{ei}} u_{i,xx}, \tag{6}$$

$$m_i^m = m_i^{\text{Max}} + m_i^{\text{Lor}} = \frac{B_0^2 b h_i}{\mu_0}\left(\frac{\pi}{2\ln\frac{x}{L-x}}u_{i,x} - \frac{h_i}{2\pi}w_{,xx}\ln\frac{x}{L-x} + w_{,x}\right) - \frac{B_0^2 h_i^3}{12\mu_{ei}}w_{,xxx}, \tag{7}$$

where b is the width of sandwich beam, $h_i\,(i = t, b)$ are the thickness of top and bottom skins, $\mu_{ei}\,(i = t, b)$ is the permeability of the skins, B_0 is the modulus of magnetic induction applied magnetic field, μ_0 is the magnetic permeability in free spaces, m_i^m is the equivalent moments induced by magnetoelastic loads at the top (t) and bottom (b) skins, n_i^m is the equivalent horizontal force induced by magnetoelastic loads at the top (t) and bottom (b) skins, m_i^{Max} is the equivalent moments induced by Maxwell's stress jump at the top (t) and bottom (b) skins, m_i^{Lor} is the equivalent moments induced by Lorenz body force at the top (t) and bottom (b) skins.

The virtual quantities δu_1 and δu_3 on the one hand and δw on the other which are expressed as follows:

$$\int_0^L \left[N_1\delta u_{1,x} + G_{\text{c}} b\gamma_{\text{c}}\delta u_1\right]\mathrm{d}x = 0, \tag{8}$$

$$\int_0^L \left[N_3\delta u_{3,x} + G_{\text{c}} b\gamma_{\text{c}}\delta u_3\right]\mathrm{d}x = 0, \tag{9}$$

$$\int_0^L \left[EIw_{,xx}\delta w_{,xx} + \left(N_1 + N_2\right)w_{,x}\delta w_{,x} + G_{\text{c}} b h_2\gamma_{\text{c}}\delta w_{\text{c}}\right] \mathrm{d}x - F_m\delta w(0) + \delta U = 0, \tag{10}$$

where $\delta U = -(q_1\delta w + n_1\delta u_1 + m_1\delta w_{,x} + q_3\delta w + n_3\delta u_3 + m_3\delta w_{,x})$.

The boundary conditions of the beam are given as follows:fixed edge: $w(0) = w_{,x}(0) = u_{1x}(0) = u_{3x}(0) = \theta_z(0) = 0$,free edge: $M_z(L) = EI_z w_{,xx}(L) = 0$.

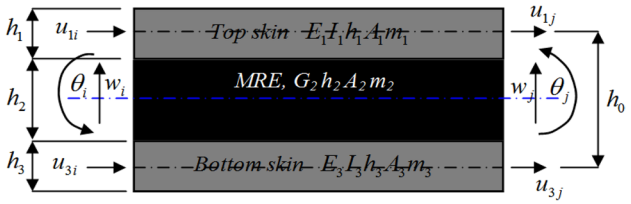

Fig. 2 Finite element model for the damped sandwich beam

3 Finite element formulation

3.1 The displacement description

The finite element model of the damped three-layer beam is shown in Fig. 2. It is assumed that every layer has the same transverse displacement, as has been proved by both numerical and experimental analysis, and that the deformation of the face sheets obeys thin plate theory, where A_i and m_i are the cross-sectional area and mass per unit length of the i^{th} layer of the beam element.

At each node n, four displacements $\{q_n\}$ are introduced, these being the transverse displacement w_n, the rotation θ_n of the elastic layers (or face sheets), and the axial displacements u_{n1}, u_{n3} of the middle planes of these face sheets. The total set of nodal displacements for the element is

$$\{q^e\} = \begin{Bmatrix} q_i \\ q_j \end{Bmatrix} = \begin{bmatrix} w_i & \theta_i & u_{1i} & u_{1j} & w_j & \theta_j & u_{3i} & u_{3j} \end{bmatrix}, \tag{11}$$

with the traditional polynomial shape functions, the displacement field vector $\{\delta\}$ may be written as

$$\{q^{\text{e}}\} = \begin{Bmatrix} w \\ \theta \\ u_1 \\ u_3 \end{Bmatrix} = \begin{Bmatrix} N_f \\ N_f' \\ N_1 \\ N_3 \end{Bmatrix}, \tag{12}$$

where

$$\begin{bmatrix} N_1 \end{bmatrix} = \begin{Bmatrix} 0 & 0 & 1-\xi & 0 & 0 & 0 & \xi & 0 \end{Bmatrix}, \tag{13a}$$

$$\begin{bmatrix} N_3 \end{bmatrix} = \begin{Bmatrix} 0 & 0 & 0 & 1-\xi & 0 & 0 & 0 & \xi \end{Bmatrix}, \tag{13b}$$

$$[N_f] = \left\{ 1-3\xi_2+2\xi \;\; (\xi-2\xi_2+\xi_3)L \;\; 0 \;\; 0 \;\; 3\xi_2-2\xi_3 \;\; (-\xi_2+\xi_3)L \;\; 0 \;\; 0 \right\}, \tag{13c}$$

with $\left[N_f'\right] = \frac{\partial N_f}{\partial x}$ and $\xi = \frac{x}{L}$ whether $x = 0 \Rightarrow \xi = 0$, $x = L \Rightarrow \xi = 1$.

3.2 Stiffness matrix for the face sheets

To discretize the two aluminum parts, we used a beam element with two nodes by fixing the characteristic length of the finite elements to $l_{\text{e (skins)}} = 0.1$ mm, each node has four degrees of freedom (Fig. 2), the stiffness matrix for the elastic face sheets may be obtained from the bending and extensional train energies as follows:

$$\begin{aligned} U &= \frac{1}{2}\int_V \left(\varepsilon_1\sigma_1 + \varepsilon_3\sigma_3\right)\mathrm{d}V = \frac{1}{2}\int_0^L \left(E_1A_1\left(\frac{\partial u_1}{\partial x}\right)^2 + E_3A_3\left(\frac{\partial u_3}{\partial x}\right)^2 + \left(E_1A_1 + E_3A_3\right)\left(\frac{\partial^2}{\partial x^2}\right)^2 \right)\mathrm{d}x, \\ &= \frac{1}{2}\{q^e\}^T \int_0^L \left(\frac{E_1L_1}{L}\left[N_1'\right]^T\left[N_1'\right] + \frac{E_3L_3}{L}\left[N_3'\right]^T\left[N_3'\right] + \frac{EI}{L^3}\left[N_f''\right]^T\left[N_f''\right] \right)\mathrm{d}\xi\{q^e\}, \\ &= \frac{1}{2}\{q^e\}^T\left[K_{qq}\right]^e_{\text{face}}\{q^e\}, \end{aligned} \tag{14}$$

$$\left[K_{qq}\right]_{\text{face}} = \begin{bmatrix} \frac{12EI}{L^3} & & & & & & & \\ \frac{6EI}{L^2} & \frac{4EI}{L^2} & & & & & & \\ 0 & 0 & \frac{E_1A_1}{L} & & & & & \\ 0 & 0 & 0 & \frac{E_3L_3}{L} & & & & \\ \frac{-12EI}{L^3} & \frac{-6EI}{L^2} & 0 & 0 & \frac{12EI}{L^3} & & & \\ \frac{6EI}{L^3} & \frac{2EI}{L} & 0 & 0 & -\frac{E_3A_3}{L} & \frac{4EI}{L} & & \\ 0 & 0 & -\frac{E_1A_1}{L} & 0 & 0 & 0 & \frac{E_1A_1}{L} & \\ 0 & 0 & 0 & -\frac{E_3A_3}{L} & 0 & 0 & 0 & \frac{E_3A_3}{L} \end{bmatrix}, \tag{15}$$

where $EI = E_1L_1 + E_3L_3$.

3.3 Stiffness matrix for the core layer

To ensure good convergence of solutions in the MRE part, a comparative study of the finite elements is carried out.

In this figure, it is observed that the quadratic elements allow a very good approximation of the solution; the mesh with Q4 or Q8 leads to an error less than 0.3% on the static response. Although the quadratic elements significantly increase the size of the model, with equal number of degrees of freedom, they are more precise, which justifies their use in this work for the modeling of beam provided with a MRE core.

In this work, we chose to model the aluminum layers of the beam with solid elements. However, the use of solid finite elements for modeling the MRE layer can lead to a blocking phenomenon, and lead to a nonphysical response, so we did a test to determine what kind of finite elements it is best to use to avoid this phenomenon. Several finite elements are tested: two-node beam elements (N2), three-node beam elements (N3), four-node quadrilateral (Q4) and eight-node quadrilateral (Q8), as well as several meshes. For each finite element of mesh, the static response of the structure is calculated. The results are

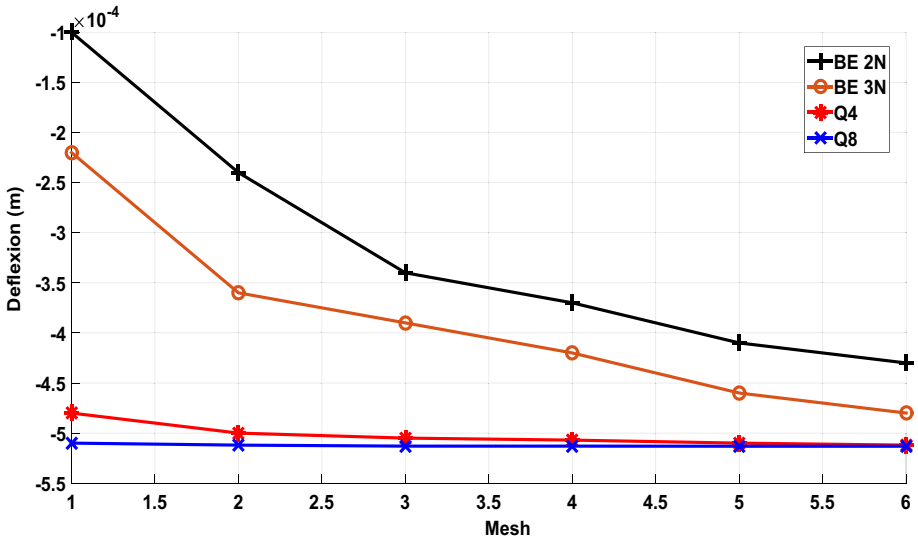

Fig. 3 Comparative study of static responses of the clamped-free beam for each finite element mesh considered

shown in Fig. 3. To ensure good continuity of movements, the proper transition and consistency between the two types of mesh elements, we have increased the size of the MRE core mesh element relative to the size of the two-part aluminum mesh element ($l_{e\,(\mathrm{MRE})} = 2l_{e\,(\mathrm{skins})} = 0.2$ mm).

The stiffness matrix of the constrained damping layer can be obtained from its shear strain energy. Here the bending and extensional strain energies are ignored due to their second-order smallness compared with the shear strain energy. It can be seen that the shear deformation is given by

$$\gamma_2 = -\frac{u_1 - u_3}{h_2} - \frac{h_0}{h_2}\theta = \frac{u_1 - u_3}{h_2} + \frac{h_0}{h_2}\frac{\mathrm{d}w}{\mathrm{d}x}, \tag{16}$$

$$\gamma_2 = -\left[\frac{N_1 - N_2}{h_2} + \frac{h_0}{h_2}\frac{\mathrm{d}N_f}{\mathrm{d}x}\right]\{q^e\}, \tag{17}$$

$$U_{\mathrm{core}} = \frac{1}{2}\int_V G_2\gamma_2^2 \mathrm{d}V = \frac{1}{2}\frac{G_2A_2L}{h_2^2}\{q^e\}^T\int_0^1\left[N_1 - N_3 + \frac{h_0}{L}N_f'\right]^T, \tag{18}$$

$$U_{\mathrm{core}} = \frac{1}{2}\{q^e\}^T\left[K_{qq}\right]^e_{\mathrm{core}}\{q^e\} \tag{19}$$

$$\left[K_{qq}\right]^e_{\mathrm{core}} = \frac{G_2A_2L}{h_2^2}\begin{bmatrix} \frac{6h_0^2}{5L^2} & & & & & & \\ \frac{h_0^2}{10L} & \frac{2h_0^2}{15} & & & & & \\ -\frac{h_0}{2L} & \frac{h_0}{12} & \frac{1}{3} & & & & \\ \frac{h_0}{2L} & -\frac{h_0}{12} & -\frac{1}{3} & \frac{1}{3} & & & \\ \frac{6h_0^2}{5L^2} & -\frac{h_0^2}{10L} & \frac{h_0}{2L} & -\frac{h_0}{2L} & \frac{6h_0^2}{5L^2} & & \\ \frac{h_0^2}{10L} & -\frac{h_0^2}{30} & -\frac{h_0}{12} & \frac{h_0}{12} & \frac{h_0^2}{10L} & \frac{2h_0^2}{15} & \\ -\frac{h_0}{2L} & -\frac{h_0}{12} & \frac{1}{6} & -\frac{1}{6} & -\frac{h_0}{2L} & \frac{h_0}{12} & \frac{1}{3} \\ \frac{h_0}{2L} & \frac{h_0}{12} & -\frac{1}{6} & \frac{1}{6} & -\frac{h_0}{2L} & -\frac{h_0}{12} & -\frac{1}{3} & \frac{1}{3} \end{bmatrix}, \tag{20}$$

where the complex modulus varies depending on the frequency of the intensity of the magnetic field and the elemental stiffness matrix for the constrained layer beam element is

$$\left[K_{qq}\right]^e = \left[K_{qq}\right]^e_{\mathrm{face}} + \left[K_{qq}\right]^e_{\mathrm{core}}. \tag{21}$$

Finally, equation set can be written in matrix notation:

$$\left[K_{qq}\right]^e\{q^e\} = \{F\} + \left\{\tilde{F}\right\}, \tag{22}$$

where $\left[K_{qq}\right]^e$ symbolizes the global stiffness matrix, $\{F\}$ external magnetic force vector, $\left\{\tilde{F}\right\}$ magnetic force vector (horizontal force distribution and the distributed moments). Solved problem example in the experimental is used to compare this developed solution. Presented solutions are compared to solve problems with the same material specifications, loading and geometric conditions. Material properties are formulated with the help of Prony Series. Integral expressions in the calculation of stiffness matrix elements are integrated by the means of two different methods for Timoshenko beam. Integral operations of terms which express bending rigidity are executed with full integration method, and reduced integration method is used for terms of shear rigidity. The purpose is the elimination of shear rigidity dominancy in the solution, and avoid from divergence called locking during the solution. If the behavior of the beam is investigated according to different $\frac{L}{h}$ ratio, the aforementioned locking can occur. Reduced integration is used with Gauss–Legendre Rule method to overcome that problem. Matrix manipulation operations are executed with Matlab program, mentioned above, and numerical method developed by Honig and Hirdes is used for reverse Laplace transformation.

3.4 Numerical simulation

The current formulation is developed to study the static analysis of a sandwich beam with MRE core. The MER core is sandwiched between two aluminum layers. The beam is clamped at one end and a magnetic variable force F_m is applied at the free end (Fig. 4). Material specifications are exactly the same as in the experimental part (Tables 1, 2). Geometrical properties of the beam are length $L = 150$ mm,

Table 1 Material properties of sandwich beam with MRE core

Property	Aluminum	MRE core
E (MPa)	72,000	1.7
ν	0.34	0.44
ρ (kg/m^3)	27,000	1100
μ_e (Hm^{-1})	1.2566650×10^{-6}	–

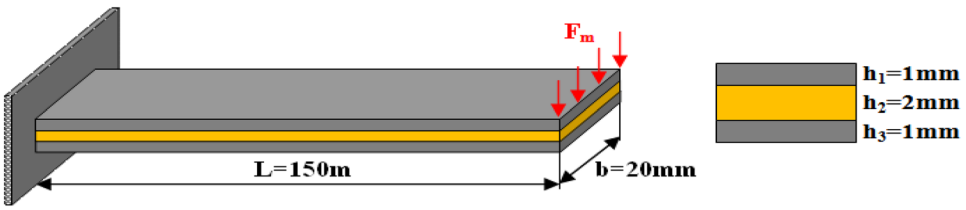

Fig. 4 Geometry of the studied structure for the comparative analysis of the elements concerning the blockage in shear

Table 2 Experimental properties MRE core at $f = 100$ Hz, $T = 27$ °C

$B = 0$ T		$B = 0.5$ T		$B = 1$ T		$B = 1.5$ T	
G' (MPa)	G'' (MPa)	G' (MPa)	G'' (MPa)	G' (MPa)	G'' (MPa)	G' (MPa)	G'' (MPa)
1.6	0.33	2.07	0.35	2.3	0.4	2.7	0.46

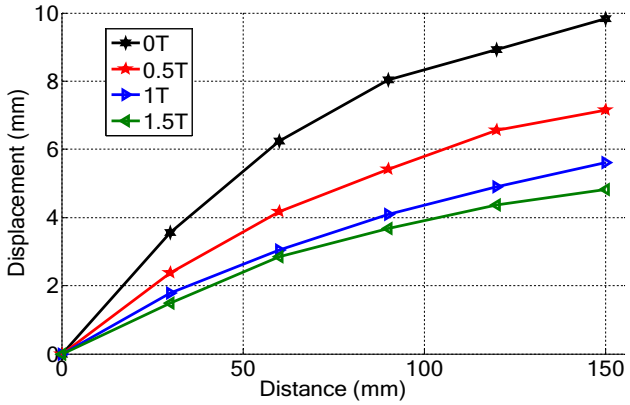

Fig. 5 Displacement distance variation curve for various magnetic field intensity

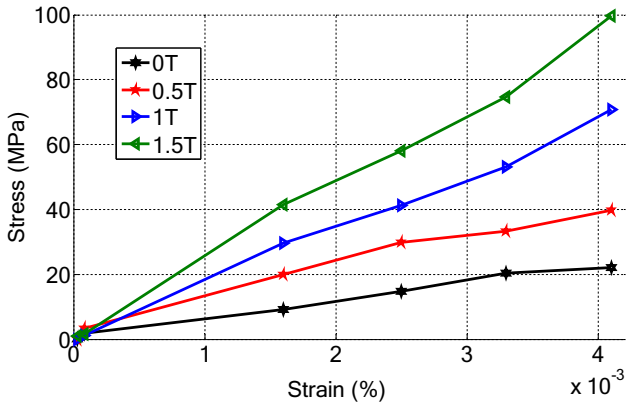

Fig. 7 Stress–strain curves during the deformation sandwich beam for various magnetic field intensity

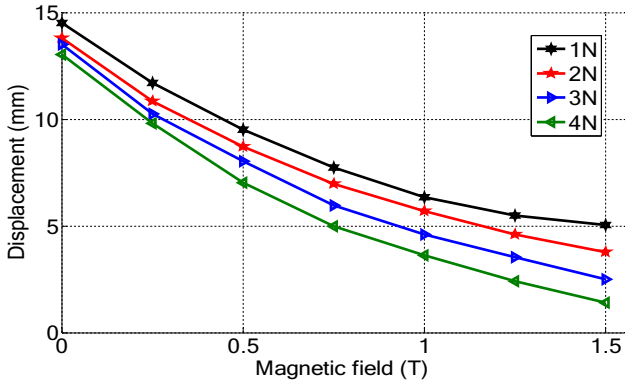

Fig. 6 Displacement magnetic field intensity variation curve for various applied force F_m

face sheet thickness $h_1 = h_3 = 1$ mm, and core thickness $h_2 = 2$ mm.

The knowledge of dynamic properties is needed especially for materials that are used in equipment subjected to vibration such as in aerospace and automotive industries. To describe the efficiency of damping, parameters such as the shear modulus G^*, consisting of the storage modulus G' and loss modulus G'' are used, determined by rheological tests.

Figure 5 shows the variation of transverse displacement versus distance of the beam with a magnetic field varied as 0, 0.5, 1, and 1.5 T with an $F_m = 1$ N. The displacements are obtained, we use the present formulation are varied in function of the variation of magnetic field intensity. We can observe that the displacement decreases with the magnetic field intensity increase because of the increase of stiffness of MRE with increasing of attractive force between the iron particles. We note that the arrow is reduced by 60% by comparing between the curve obtained for $B = 0$ T and the curve obtained for $B = 1.5$ T.

Figure 6 represents the variation of transverse displacement versus magnetic field intensity under the excitation of an attractive magnetic force F_m varied as 1, 2, 3 and 4 N. The displacements decrease as the increasing of magnetic field intensity; because, the increasing of magnetic field caused the increasing of two modulus G' and G'', the biggest values of G' and G'' are obtained in a magnetic field intensity of 1.5 T. Inversely, the displacements increase with the increasing of attractive magnetic force F_m. We observe that for a value of $B = 1.5$ T we have a displacement of 5.03 mm for $F_m = $ N; 3.77 mm for $F_m = 3$ N; 2.55 mm for $F_m = 2$ N, and 1.4 mm for $F_m = 1$ N. It is noted that the arrow is reduced by 40% by comparing between the curve obtained for $F_m = 1$ N and the curve obtained for $F_m = 4$ N.

Figure 7 represents the variation of the stress–strain curve of the beam as a function of different intensities of the magnetic field. We can observe that the stress varied proportionally with magnetic field intensity, the MRE stiffness increase with the increasing of magnetic field intensity, so the MRE under a magnetic field is characterized by an increasing of it stiffness as the resistance in the compression result of the attractive force created between the iron particles. Otherwise, we observe that the top level of stress–strain curve is

for the maximum MFI $B = 1.5$ T and the higher anisotropic of MRE. It is noted that the stress increases by 400% by comparing between the curve obtained for $B = 0$ T and the curve obtained for $B = 1.5$ T.

Thus, this study provides a finite element model able to take into account these specificities of MRE and gives good flexibility and efficiency for modeling rheological complex materials. The second advantage is the implementation of techniques and calculations. In the code developed in Matlab, we exploited the symmetry of the rigidity matrix; this ensured the continuity of stress–displacement and reduced computation time with a substantial memory gain. Indeed, it stores only the half-band and the diagonal of the matrix by taking advantage of symmetry.

4 Conclusions

In this paper, a nonlinear static analysis of composite beams with the core in magnetorheological elastomer was carried out using the finite element method (FEM). The clamped-free boundary conditions were considered. Conclusions that can be drawn are as follows:

It is found that the deflection of the beam sandwich increases with the increase of the applied magnetic force to the free edge.

The deflection of the beam sandwich decreases with increase in the intensity of the magnetic field.

The results found showed that the magnetorheological elastomer exhibits a highly non-linear behavior from a mathematical and material point of view.

This study shows a progress in the manufacture of low-cost damping elements with great flexibility in the design and in the variation of the static behavior as a function of the variation of the mechanical characteristics of the magnetorheological elastomer subjected to different intensity of the magnetic field.

References

1. G.Y. Zhou, Q. Wang, Use of magnetorheological elastomer in an adaptive sandwich beam with conductive skins, Part I: magnetoelastic loads in conductive skins. Int. J. Solids Struct. **43**, 5386–5402 (2006)
2. G.Y. Zhou, Q. Wang, Use of magnetorheological elastomer in an adaptive sandwich beam with conductive skins. Part II: dynamic properties. Int. J. Solids Struct. **43**, 5403–5420 (2006)
3. Y. Wan, Y. Xiong, S. Zhang, Temperature dependent dynamic mechanical properties of magnetorheological elastomers: experiment and modeling. Compos. Struct. **202**(15), 768–773 (2018)
4. A.K. Bastola, M. Paudel, L. Lia, Development of hybrid magnetorheological elastomers by 3D printing. Polymer **149**, 213–228 (2018)
5. J. Yao, Y. Sun, Y. Wang, Q. Fu, Z. Xiong, Y. Liu, Magnet-induced aligning magnetorheological elastomer based on ultra-soft matrix. Compos. Sci. Technol. **162**(7), 170–179 (2018)
6. M. Touron, J.Y. Dieulot, J. Gomand, P.J. Barre, A port-Hamiltonian framework for operator force assisting systems: application to the design of helicopter flight controls. Aerosp. Sci. Technol. **72**, 493–501 (2018)
7. A. Dargahi, R. Sedaghati, S. Rakheja, On the properties of magnetorheological elastomers in shear mode: design, fabrication and characterization. Compos. Part B Eng. **159**, 269–283 (2019)
8. H. Akhavan, M. Ghadiri, A. Zajkani, A new model for the cantilever MEMS actuator in magnetorheological elastomer cored sandwich form considering the fringing field and Casimir effects. Mech. Syst. Signal Process. **121**, 551–561 (2019)
9. A. Dargahi, S. Rakheja, R. Sedaghati, Development of a field dependent Prandtl–Ishlinskii model for magnetorheological elastomers. Mater. Des. **166**, 107608 (2019)
10. N.T. Lai, H.M. Ismail, K. Abdullah, R.K. Shuib, Optimization of pre-structuring parameters in fabrication of magnetorheological elastomer. Arch. Civ. Mech. Eng. **19**(2), 557–568 (2019)
11. X. Xing, J. Liu, L. Wang, Modeling and vibration control of aero two-blade propeller with input magnitude and rate saturations. Aerosp. Sci. Technol. **84**, 412–430 (2019)
12. M. Z. Aşık, S. Tezcan, A mathematical model for the behavior of laminated glass beams. Comput. Struct. **83**(21–22), 1742–1753 (2005)
13. M.G. Sainsbury, Q. J. Zhang, The Galerkin element method applied to the vibration of damped sandwich beams. Comput. Struct. **71**(3), 239–256 (1999)

Salah Aguib received HDR degree in Mechanical Engineering Institute from Boumerdes University, Algeria, in 2014. His researches have been based on vibration control of mechanical structures and dynamic systems by smart materials.